6 February 2020

For *Journal of Hydrology*

Application of time domain reflectometry to high suspended sediment concentration measurements: laboratory validation and preliminary field observations in a steep mountain stream

Short title: Application of TDR to high sediment transport.

Shusuke Miyata[1], Shigeru Mizugaki[2], Shuya Naito[3], and Masaharu Fujita[1]

[1] Disaster Prevention Research Institute, Kyoto University, Japan

[2] Civil Engineering Research Institute for Cold Region, Public Works Research Institute, Japan

[3] CTI Engineering Co., Ltd., Japan

Key points:

- A time domain reflectometry (TDR) system is proposed, with a straightforward calibration procedure consisting of a single measuring device and multiple coil-type sensor probes, enabling the measurement of vertical sediment concentration distributions in streams.
- Laboratory tests validated the suspended-sediment concentrations with an accuracy of ± 0.01 $m^3\ m^{-3}$ for practical use.
- During a hazardous storm, the sediment concentration increased by up to 0.07 $m^3\ m^{-3}$ at peak discharge, and high sediment concentrations of approximately 0.4 $m^3\ m^{-3}$ at various heights indicated the potential for deposition in a steep stream.

Abstract

The dielectric constant around a sensor was measured with a time domain reflectometry (TDR) system and used to calculate the volumetric sediment concentration (SC) of stream water and deposition on a streambed. The measurements of various SCs in laboratory experiments demonstrated that the TDR system proposed in this study had an accuracy of 0.01 m^3 m^{-3} for practical uses, and that the measured concentrations were not sensitive to particle size. The vertical SC distributions were measured at heights of 17–37 cm in a steep mountain stream. The resulting SCs at the various heights increased by 0.01–0.07 m^3 m^{-3} at the time of peak stream discharge during an extreme storm with a return period of approximately 12 years. After extreme precipitation, the SC of the lowest probe increased rapidly from approximately 0 to 0.4 m^3 m^{-3}. This was followed by rapid increases in the SCs at the other heights, indicating deposition around each probe. The TDR measurement system, with its straightforward calibration procedure, effectively measured deposition and a high-concentration layer above the deposited layer even during the storm event.

Keywords: TDR; water and sediment mixture; suspension; streambed elevation; hazardous storm

1. Introduction

Suspended sediment consists of fine sediment particles suspended in a stream flow and accounts for a substantial amount of the total sediment transport in high-gradient fluvial environments (Lenzi et al., 2003; Turowski et al., 2010; Kociuba, 2017; Piqué et al., 2018). An assessment of sediment transport rates in a channel network is important for understanding fluvial dynamics (Dietrich et al., 1989; Buffington and Montgomery, 1997), sediment production in catchments (Lenzi et al., 2003) and estimating the runoff of nutrients and pollutants associated with suspended sediments (Walling and Collins, 2008; Hostache et al., 2014). Optical turbidimeters are widely used for in situ measurements of the sediment concentration (SC) of suspensions (Wren et al., 2000; Gray and Gartner, 2009; Rai and Kumar, 2015). Multiplying stream discharge and the SC measured by a turbidimeter gives a time series of suspended sediment transport at a certain cross section.

The advantages of turbidity-based measurement techniques (i.e., optical turbidimeters) are the ease of installation and established standards for operation, while turbidimeters have limitations such as dependences on the size, colour and shape of suspended particles, ability to make point measurements and biological stains changing the calibration curves (Rai and Kumar, 2015). The upper SC limits of turbidimeters are reported to be 2 g L^{-1}, corresponding to a volumetric SC of approximately 7.5×10^{-4} m^3 m^{-3}, for clay and silt particles, but are greater for sand (Gray and Gartner, 2009). By contrast, very high suspended SCs, i.e., greater than 7.5×10^{-4} m^3 m^{-3}, have been recorded in alpine streams (Turowski et al., 2010; García-Mama et al., 2016; Felix et al., 2018; Comiti et al., 2019), mountain streams (Abe et al., 2012; Chung et al., 2013a) and arid ephemeral streams (Cohen and Laronne, 2005). When the suspended SC exceeds the measurement range of a turbidimeter, critical SC information during specific events is lost

66 (Voichick et al., 2018). Therefore, a combination of a turbidimeter for lower SCs and other
67 measurement techniques for higher SCs is advisable to cover the low- to high-flow conditions.
68 The application of time domain reflectometry (TDR) to suspended SC measurements has
69 recently been proposed (Starr et al., 2000; Chung and Lin, 2011; Mishra et al., 2018). A TDR
70 measurement yields a dielectric constant, which is a composition of the dielectric constants of
71 materials surrounding the sensor probe (Černý, 2009). Laboratory measurements of suspended
72 SC have revealed that the TDR approach is effective for SCs greater than 7.5×10^{-4} m^3 m^{-3} (Chung
73 and Lin, 2011). An SC measurement using a TDR device also has the advantage of being
74 insensitive to sediment particle size (Chung and Lin, 2011), whereas the conversion of measured
75 turbidity into SC strongly depends on the particle size distribution (Wren et al., 2000; Gray and
76 Gartner, 2009; Rai and Kumar, 2015). Because coarser particles can be transported as suspensions
77 during huge floods with large shear stresses (Walling et al., 2000), the TDR method can be used
78 to observe suspended sediment transport during such events.
79 Extreme floods often cause changes in streambed elevation (i.e., sedimentation and scouring;
80 Laronne et al., 1994; Martin and Church, 1995; Lane et al., 2007; Martín-Vide et al., 2019). It is
81 difficult to monitor sediment transport during such extreme flood conditions because the sensors
82 for suspended SC measurement are at a risk of malfunction due to sedimentation.
83 The measurement of vertical and/or cross-sectional distributions of SC in stream flow by
84 TDR measurements is likely to be possible using multiple sensors. Multiple sensor probes can be
85 connected to one single TDR device (e.g., Heimovaara and Bouten, 1990; Persson and Dahlin,
86 2010; Miyata and Fujita, 2018). Such multi-measurements expand the volume to be measured,
87 which is essential for the accurate evaluation of suspended sediment transport. The TDR sensor
88 can be manufactured at low cost (Miyata and Fujita, 2018), offering an economical advantage

89 when installing multiple TDR sensors to observe SC distributions. Thus, the TDR method with
90 multiple sensor probes can be suitable for observations of the SC distribution in mountain streams,
91 in which the water levels can change greatly due to sedimentation and scouring (Laronne et al.,
92 1994; Martin and Church, 1995; Lane et al., 2007; Martín-Vide et al., 2019).

93 Although TDR has recently been found to be an effective approach for measurements of very
94 high suspended SC (Starr et al., 2000; Chung and Lin, 2011; Mishra et al., 2018), only a few
95 applications in the field observation of suspended SC have been reported (e.g., Starr, 2005; Chung
96 et al., 2013a). In this study, we used the TDR approach to assess SCs in stream water. The
97 measurement method was validated using laboratory experiments. To demonstrate the
98 performance of the method, we present the preliminary results from field observations during an
99 extreme storm event.

100

101 **2. Theoretical background**

102 A typical TDR measurement system consists of a cable tester and transmission line (Fig. 1).
103 An electromagnetic wave pulse generated by the cable tester propagates the transmission line and
104 is reflected at the end of the line. The transmission line consists of a coaxial cable and probe that
105 acts as the system's sensor and is embedded in the target material. Primary measurements appear
106 as a waveform representing the reflection coefficient and apparent distance, which is the product
107 of time and the velocity of light. The travel time of the electromagnetic wave depends on the
108 dielectric constant ε of the material around the probe, which is calculated using the following
109 equation:

110 $$\varepsilon = \left(\frac{ct}{L}\right)^2 = \left(\frac{L_a}{LV_p}\right)^2 \quad (1)$$

111 where t is the one-way travel time of the electromagnetic wave propagating in the transmission

112 line; c is the velocity of light (2.99×10^8 m s^{-1}), which is equal to that of the electromagnetic
113 wave in a vacuum; L_a is the apparent length of the probe; L is the actual probe length; and V_p is
114 the propagation velocity coefficient of the transmission line (0.99 in this study).

115 Because turbid stream water can be assumed to consist of water and sediment particles, the
116 dielectric constant of the turbid water can be calculated using the volumetric mixing model
117 proposed by Dobson et al. (1985). The square root of the complex dielectric constant of the turbid
118 stream water ε_{obs} is calculated using the dielectric constants of water ε_w and the sediment
119 particles ε_s, as follows:

120 $$\sqrt{\varepsilon_{obs}} = (1 - C)\sqrt{\varepsilon_w} + C\sqrt{\varepsilon_s} \quad (2)$$

121 where C is the volumetric SC. The dielectric constant of water is 78.3 at 25°C and depends on the
122 water temperature (Malmberg and Maryott, 1956). We used a value of 3.0 for ε_s, based on the
123 known values of 2.5–3.5 for sand (Noborio, 2001). The volumetric concentration is expressed as:

124 $$C = \frac{\sqrt{\varepsilon_{obs}} - \sqrt{\varepsilon_w}}{\sqrt{\varepsilon_s} - \sqrt{\varepsilon_w}} \quad (3)$$

125

126

127 **3. Materials and methods**

128 **3.1 Measurement system and probe design**

129 The SC of water was measured using a measurement system composed of a data logger
130 (CR1000; Campbell Scientific, Logan, UT, USA), cable tester (TDR100; Campbell Scientific),
131 multiplexer (SDM50; Campbell Scientific), coaxial cables and sensor probes (Fig. 2a). The
132 multiplexer enabled measurements to be made by multiple probes with a single cable tester.

133 In this study, we used coil-type TDR probes (Figs. 2a–c), although various types of probes
134 have been proposed (Topp et al., 1980; Heimovaara, 1994; Bittelli et al., 2004; Chung et al.,

2013b; Miyata and Fujita, 2018). Because a longer waveguide is associated with higher measurement resolution (Chung and Lin, 2011), the coil-type probe has the advantage of high measurement resolution with a small probe size (Nissen et al., 1998). Two stainless-steel lines, each approximately 1.1 m in length and 0.55 mm in diameter, were rolled up and placed inside a polyvinyl chloride (PVC) pipe to act as a waveguide (Fig. 2a). The ends of the two stainless-steel lines were connected with a coaxial cable and the connection was positioned inside the PVC pipe. The cavity of the pipe was sealed to prevent the intrusion of water.

Primary measurement results (i.e., TDR waveforms) required the analysis procedure to obtain the apparent probe lengths, L_a in Eq. (1). In this study, we employed the dual tangent method, which is one of the main methods used to determine the positions of the beginning and end of a probe in a TDR waveform (Robinson and Friedman, 2003; Bittelli et al., 2004; Chung and Lin, 2011). The beginning and end of the probe were determined as the intersects of tangential lines with maximum and minimum slopes.

3.2 Probe calibration

Despite the advantage of high measurement resolution offered by the coil-type probe, prior calibration procedures are necessary to obtain the two unknown parameters of the net lengths of the stainless-steel lines and the effects of the PVC pipe. The net lengths of the stainless-steel lines acting as the sensor of the measurement system, L in Eq. (1), are difficult to determine physically. Because the two stainless lines are in contact with the PVC pipe as well as with the surrounding materials (i.e., turbid water in this study; Fig. 2d), the resulting dielectric constants include the effects of the PVC pipe (Miyata and Fujita, 2018). The dielectric constant of PVC in Eq. (2) requires an additional term to obtain the effects of the PVC pipe, as follows:

158 $$\sqrt{\varepsilon_{obs}} = \alpha\sqrt{\varepsilon_{PVC}} + (1-\alpha)\{(1-C)\sqrt{\varepsilon_w} + C\sqrt{\varepsilon_s}\} \quad (4)$$

159 where α is the constant coefficient representing the effect of the PVC pipe; and ε_{PVC} is the
160 dielectric constant of PVC (3.0 in this study; Ghodgaonkar et al., 1989).

161 TDR measurements were made using each coil-type probe for deionised water and air to
162 obtain the two unknown parameters, L and α. The dielectric constant of water ε_w is a function
163 of the water temperature (Malmberg and Maryott, 1956), and the dielectric constant of air ε_a is
164 1.0. The resulting apparent lengths in water L_{a_w} and air L_{a_a} were substituted into Eq. (1) to
165 calculate the dielectric constants, ε_{obs_w} and ε_{obs_a}, respectively, using the following equations:

166 $$\frac{L_{a\_w}}{LV_p} = \sqrt{\varepsilon_{obs\_w}} = \alpha\sqrt{\varepsilon_{PVC}} + (1-\alpha)\sqrt{\varepsilon_w} \quad (5a)$$

167 $$\frac{L_{a\_a}}{LV_p} = \sqrt{\varepsilon_{obs\_a}} = \alpha\sqrt{\varepsilon_{PVC}} + (1-\alpha)\sqrt{\varepsilon_a} \quad (5b)$$

168 From Eqs. (5a) and (5b), the net length of the stainless-steel line, L, and the coefficient of the
169 effects of the PVC pipe, α, were obtained.

170 These calibration procedures were followed for the five coil-type probes used in the
171 laboratory experiments described in the following section. The calculated values of L and α varied
172 slightly among the five probes, ranging from 1.13 to 1.15 m and 0.244 to 0.263, respectively
173 (Table 1). These slight variations confirmed the homogeneity of the handmade sensors. The
174 calibration procedures were straightforward and easy to perform.

175

176 **3.3 Laboratory experiments for validation**

177 The proposed system was validated with two series of laboratory experiments: the TDR
178 measurements were performed for deionised water (experiment I) and various SCs of turbid water
179 (experiment II; Fig. 3). In experiment I, repeated TDR measurements of deionised water were

made to evaluate the variation in resulting concentrations. The calibrated coil-type probes A–E and a thermometer were used in these repeated measurements (Table 2).

The calibrated coil-type probes, a three-rod probe and a thermometer were embedded in 60 L of deionised water in experiment II (Fig. 3). The three-rod probe, with a 30 cm rod length, is commonly used for soil water measurement (Noborio, 2001), and its performance was compared with the coil-type probes. Sand was added to the water and mixed well during the measurements using a hand mixer. At each concentration level, two or three repeat measurements were made by all probes. The experiments were conducted with two different particle sizes. Silica sand #7 consisting of particles with a mean diameter of 0.2 mm was used in Run II-1, and kaolin clay, with a uniform particle size (mean diameter of 0.0004 mm) was used in Run II-2 (Table 2 and Fig. 4). The dielectric constants of both sand and kaolin clay were assumed to be 3.0. The maximum volumetric concentrations in Runs II-1 and II-2 were 0.113 and 0.151 $m^3\ m^{-3}$, respectively, corresponding to mass concentrations of 300 and 400 g L^{-1}, respectively. The five coil-type probes (probes A–E) were used in Run II-1, whereas only three probes (probes B–D) were used in Run II-2.

3.4 Field observations

The TDR system was installed in a steep mountain stream, the Soshubetsu River, which is a tributary of the Saru River, in northern Japan (Fig. 5a). The river width, average gradient and drainage area at the monitoring station were 25 m, 0.065 and 16.7 km^2, respectively. The study catchment was mostly covered by forest. The annual precipitation in the study area, including snow, is 1,182 mm, as measured at Asahi meteorological station, which is 4 km south of the study site (Fig. 5a). The study catchment is covered by snow during winter. The annual maximum snow

203 depth at Asahi meteorological station ranged from 0.22 to 0.75 m from 2004 to 2016.

204 The study site experienced an extreme flood in August 2003 due to the passage of Typhoon
205 Etau, which brought 400 mm of precipitation and caused more than 4,000 landslides in the Saru
206 River Watershed. Less than 10% of the sediment from the landslides was transported during the
207 flood (Mizugaki et al., 2012). The residual loose sediment remained within the stream network
208 and was later transported by following storms. Continuous turbidity measurements in the study
209 catchment revealed an obvious seasonal variation of the suspended sediment transport (Abe et al.,
210 2012). The suspended sediment transport was lower during winter with less precipitation and
211 snow cover and higher due to snowmelt and storms in summer. The mean diameter of the
212 streambed material sampled in November 2016 (i.e., after the monitoring period of this study)
213 was 0.1 mm (Fig. 4).

214 Both sides of the riverbank at the monitoring station were covered with concrete blocks, whereas
215 the streambed was not protected. A pressure-type water level gauge (S&DL mini; OYO
216 Corporation, Tokyo, Japan) and turbidimeter (ATU75W2-USB; JFE Advantech, Nishinomiya,
217 Japan) were packed into a protective steel cylinder and installed on the right-hand side of the bank
218 (Fig. 5b). Stream discharge was calculated using an empirical relationship, which was established
219 based on 14 measurements of water level and discharge in the field with a coefficient of
220 determination (R^2) of 0.98. The measured discharge ranged from 0.12 to 6.23 $m^3 s^{-1}$. The discharge
221 out of this range was extrapolated from the measured water level. Turbidimeter readings were
222 converted into a volumetric concentration based on the exponential relationship between turbidity
223 readings and sediment concentrations in water samples collected at the study site ($R^2 = 0.98$) (Abe
224 et al., 2012; Mizugaki et al., 2013). The water samples were collected during the snowmelt period
225 and storms in 2011 and 2012 and their sediment concentrations ranged from 7.5×10^{-8} to 2.6×10^{-3}

226 $m^3 m^{-3}$ at discharges of 0.6 to 8.0 $m^3 s^{-1}$.

227 The sensor probes of the TDR system were installed adjacent to the water level gauge and
228 turbidimeter (Fig. 5b). Five coil-type probes were fixed at heights of 17–37 cm above the
229 streambed at 5-cm intervals (Figs. 5c and d). The probes were installed without any protection
230 and were exposed directly to the stream flow. The height of the turbidimeter was 27 cm above the
231 bed, corresponding to the height of probe C-3; however, no data were retrieved from probe C-3
232 due to a failure in the system settings. A three-rod-type probe was installed at a height of 42 cm
233 for evaluation of the probe geometry. Because water temperature is known to be an important
234 factor in the calculated SC (Chung and Lin, 2011), a temperature sensor (109SS; Campbell
235 Scientific), with an accuracy of ± 0.1°C at 25°C was installed at a height of 22 cm. The vital parts
236 of the TDR system, such as the cable tester, were placed in a secure location, i.e., at the top of the
237 protective bank (Fig. 5b). The water level, turbidity and SC measured by the TDR system were
238 recorded every 10 min. Field observations of water level and turbidity began in 2010, while the
239 TDR measurements were conducted from July to August 2016.

240

241 **4. Results and discussion**

242 **4.1 Laboratory evaluations of the suspended SC**

243 The average and standard deviation of the 20 repeated measurements for deionised
244 water in Experiment I were 4.5×10^{-4} and 5.6×10^{-3} $m^3 m^{-3}$, respectively. The variation recorded
245 in our experiment was comparable to that reported by Chung and Lin (2011), who conducted
246 repeated TDR measurements for clean water using two- or three-rod probes with different lengths
247 and found SC variations of approximately $2.6 \times 10^{-3} - 1.1 \times 10^{-2}$ $m^3 m^{-3}$. The repeated
248 measurements in our experiment revealed that the TDR system equipped with the coil-type probe

249 resulted in a variation in SC values greater than that of widely used optical-type turbidimeters.

250 In Experiment II, linear regression analysis revealed significant correlations between
251 the actual SC, calculated from the volume of sand and water in the container, and the SCs
252 measured using the TDR with high determination coefficients (R^2) greater than 0.88 (Table 3; Fig.
253 6). Slopes of the regression equations ranged from 0.700 to 1.05. Intercepts of the regression
254 equations were -0.0008 – 0.022 m^3 m^{-3}, which were comparable to the standard deviation of SC
255 for deionized water (i.e., Experiment I).

256 The differences between the average value for the resulting SCs of the five coil-type
257 probes and the actual SCs ranged between −0.01 and 0.01 m^3 m^{-3}, except for a single outlier of
258 −0.011 m^3 m^{-3} in Run II-2 (Fig. 7). The averaging of the repeated SC measurements likely
259 minimised the effects of the heterogeneity of the turbid water within the container. These
260 experimental results implied an accuracy of ± 0.01 m^3 m^{-3} in the volumetric suspended SC for
261 practical use when the proposed measurement method was applied using the coil-type probe.

262 To test the effects of particle size of suspension on measurement results, analysis of
263 covariance (ANCOVA) was conducted (Table 4). There were no significant differences between
264 the averaged SCs for each concentration level of Runs II-1 and II-2. The ANCOVA results suggest
265 that measured SCs using the TDR system were not influenced by particle size, although only two
266 particle sizes were tested in this study.

267

268 **4.2 Suspended sediment concentration and subsequent deposition during a severe flood**

269 Typhoon Mindulle passed over the study site on 21–23 August 2016, bringing 243.5 mm of
270 precipitation to the area (Fig. 8). The precipitation of 243.5 mm within 72 h corresponds to a
271 return period of approximately 12 years. The protective bank at the monitoring station was

damaged due to overspill from the heavy precipitation (Fig. 9b). Approximately 0.8 m of sediment deposition was observed at the monitoring station around two weeks after the storm (Fig. 9c). Because further huge precipitation generated by another typhoon was forecasted, the vital components of the measurement system packed in the logger box were removed on 26 August.

The peak stream discharge during the event was 49 $m^3 s^{-1}$ (Fig. 8a). The turbidity reached a maximum volumetric concentration of 0.0076 $m^3 m^{-3}$ at the time of peak discharge (Fig. 8b). No turbidity data were available after 10:30 on 23 August due to sediment deposition. The SCs at probes C-1, C-2, C-4 and C-5 tended to vary in correspondence with the changes of discharge and turbidity. At the time of peak discharge and turbidity, the SCs at probes C-1, C-2, C-4 and C-5 increased by 0.02, 0.01, 0.02 and 0.07 $m^3 m^{-3}$, respectively. The largest increases in SC at probe C-5 may reflect high levels of suspended sediment transport near the flow surface. The other possible factor influencing the increased SC at probe C-5 was captured organic materials such as woody debris or leaf litter, as the dielectric constants of organic materials were comparable with those of soil particles (Woodhead et al., 2003). By contrast, at the time of the initial small peak discharge and turbidity (i.e., around 13:30 on 21 August), the increases in SCs recorded by the coil-type probes were very small and within the range of measurement accuracy. Because the SC derived from the three-rod probe contained a lot of noise, the data were omitted from the analysis presented in this section.

The SCs began to increase again as the discharge began to decrease, and finally reached a steady state value of approximately 0.4 $m^3 m^{-3}$, as measured by all the coil-type probes (Fig. 8). For example, the SCs of probe C-1 at a height of 17 cm began to increase at 10:00 on 23 August and reached 0.4 $m^3 m^{-3}$ at 16:00. All probes at heights of 17–42 cm were buried after the storm (Fig. 9c); therefore, these high SC values reflected the deposition around the probes. These high

295 SCs reflecting the deposited sediment correspond to the finding of our previous study in which
296 the sediment fractions of deposits in a model retention basin were measured using the TDR
297 technique (Miyata & Fujita, 2018). The time from the beginning of the period of increasing SCs
298 to when the SCs reached steady state values was approximately 6.0, 6.5, 11.5 and 8.5 h at C-1, C-
299 2, C-4 and C-5, respectively (Figs. 8d–g).

300 The vertical distributions of SC revealed the thickness of the deposited sediment and the high
301 SC layer above the deposited sediment (Fig. 8h). For example, at 15:30 on 23 August, the
302 observed SCs at heights of 17, 22, 32 and 37 cm were 0.39, 0.14, 0.02 and −0.01 $m^3\ m^{-3}$,
303 respectively. Assuming that SCs greater than 0.3 $m^3\ m^{-3}$ indicated sediment deposition, the SC
304 value of 0.14 $m^3\ m^{-3}$ at a height of 22 cm corresponded to the deposition surface located at around
305 the centre of the probe. Because the radius of a TDR measurement was less than 1 cm from the
306 probe surface in water (Starr et al., 2000; Bittelli et al., 2004), the resulting SC at a height of 32
307 cm was not associated with the deposited sediment but rather the suspended and/or bedload
308 sediments above the deposit. The TDR system proposed in this study was able to demonstrate the
309 deposition and existence of a high SC flow above the deposit.

310 The observed SCs displayed slight increases on 25 and 26 August 2018 (Fig. 8h). The
311 increases in SC when steady state conditions were reached at the end of the observation (9:00 on
312 26 August) were approximately 0.04, 0.03, 0.05 and 0.05 $m^3\ m^{-3}$ at C-1, C-2, C-4 and C-5 (Figs.
313 8c–g). These increases in SC potentially reflected the mechanical compaction of the deposit
314 (Houseknecht, 1987) and/or the propagation of fine particles into pores of the deposit (Núñez-
315 González et al., 2016).

316

317 **4.3 Applicability of the TDR system to field observations**

318 The TDR system was able to record SCs throughout the severe storm event on 21–23 August
319 2016 (Fig. 8), which was caused by a typhoon passing over the study site. The severe storm
320 resulted in the overspill of the flow and serious damage to the protective bank (Figs. 9b and c).
321 The sensors were robust even during such severe stream conditions. A vital part of the
322 measurement system was slightly damaged by driftwood and was removed on 26 August to avoid
323 further damage due to a forecasted typhoon approaching the study site. However, the bank and
324 logger box were not damaged and extra probes were installed above the deposited material, so we
325 were able to continue the observation for the following storm event.
326 The SCs derived from the three-rod probe were frequently affected by noise during the event
327 on 21–23 August 2016 (Fig. 8c), while the coil-type probes yielded reliable preliminary TDR
328 waveforms and resulting SCs (Fig. 11d–g). The poor data obtained from the three-rod probe were
329 associated with the shape of its probe, which easily captured woody debris. Woody debris that
330 attached to the probe surface strongly influenced the resulting SCs. Compared with the smooth
331 surface of the coil-type probes, the geometry of the three-rod probe made it vulnerable to the
332 effects of organic matter on the resulting SCs. To use three-rod probes for SC measurements, the
333 probes need to be embedded into a solid surface as proposed by Star (2005) or packed in a
334 protective cylinder like ordinary turbidimeters. Despite the calibration procedures required for a
335 coil-type probe, their high measurement resolution is advantageous for field observations.
336 Variations in SC were apparent during no-rainfall periods in the field observations (Fig. 10)
337 as well as in experiments I and II (Figs. 6 and 7). For example, the standard deviations of 144
338 resulting SC values at probes C-1, C-2, C-4 and C-5 were 0.0054, 0.0041, 0.0056 and 0.0051 m^3
339 m^{-3}, respectively, on 4 August 2016 when no turbidity was recorded and the 5-day antecedent
340 precipitation was 0 mm. Other than these typical fluctuations, significant increases in SC were

only recorded during large storms such as those on 17, 20 and 22 August (black arrows in Fig. 10).

The turbidimeter recorded responses even during small rainfall events (Fig. 10). The differences in the sensitivity of probe C-2 used in the TDR measurement at a height of 22 cm and the turbidimeter at a height of 27 cm resulted in a weak correlation throughout the entire observation period (Fig. 11). By contrast, the responses of the SC measured by probe C-2 and the turbidimeter were correlated ($R^2 = 0.59$) around the peak discharge of the severe event on 23 August. The substantial increase in SC of up to 0.008 $m^3\ m^{-3}$ measured using the turbidimeter was also detected by probe C-2, implying a potential application of the TDR system to SCs less than the practical accuracy of 0.01 $m^3\ m^{-3}$ revealed by the laboratory experiments. The results also implied that using the exact value of the dielectric constant of the suspension in the study site improved the resulting SCs. A combination of the TDR system and turbidimeter would be effective for long-term observations of the sediment transport rate, during which various types of precipitation are experienced.

Field application of the TDR system would also require periodic maintenance of the probes. We removed fine particles and algae from the probe surfaces between 11:30 and 11:40 on 10 August 2016 (Fig. 12). As a result of this probe cleaning, the average SC at probe C-2 over a 1-h period decreased from $7.4 \times 10^{-3}\ m^3\ m^{-3}$ to $-2.4 \times 10^{-4}\ m^3\ m^{-3}$. Because the turbidimeter recorded SCs of approximately 0 $m^3\ m^{-3}$, the cleaning reduced the resulting SCs by one order of magnitude. Similar decreases in SCs were found during a storm on 27–28 July 2016 (broken arrows in Fig. 10). The stream turbulence probably removed materials on the probe surfaces, resulting in the decreases in the observed SCs measured by probes C-1 and C-2.

5. Conclusion

We propose the application of TDR to measure the volumetric fraction of sediment particles in water. Because multiple sensor probes are connected to one single measurement device (i.e., a cable tester), the TDR system enables the observation of sediment concentration distributions in stream flow. A series of laboratory tests were conducted to validate the performance of the method proposed in this study. The system was then applied to field observations in a steep mountain stream during a 1.5-month period, including an extreme storm event at the end of the study period.

Repeated TDR measurements in deionised water revealed measurement fluctuations of approximately 0.006 $m^3\ m^{-3}$. Laboratory tests of various sediment concentrations up to 0.15 $m^3\ m^{-3}$ showed that the system was effective for concentrations greater than 0.02 $m^3\ m^{-3}$, with measurement errors of 0.01 $m^3\ m^{-3}$ for practical use. The experimental results indicated that sediment particle size had little effect on the resulting concentrations in turbid water. The results of the laboratory tests implied that the TDR system was appropriate for use in conditions with huge sediment transport during extreme storm events.

The field application demonstrated that the sediment concentration measurements at various heights were robust, even during a severe storm event. At the time of peak discharge during the storm event, the sediment concentrations at the probes increased from 0.01 to 0.07 $m^3\ m^{-3}$, then increased again during a recession in the discharge due to deposition, and finally reached a steady state of approximately 0.4 $m^3\ m^{-3}$. The resulting vertical distributions of concentration also implied the existence of a high concentration layer above the deposited material. Our preliminary results suggest that continuous measurements of sediment concentrations at various heights will improve the understanding of sediment transport and deposition processes in streams.

Acknowledgment

This study was supported by Grants-in-Aid from the Ministry of Land, Infrastructure, Transport and Tourism, Japan, the Japan Society for the Promotion of Science (JSPS) KAKENHI Grant Numbers JP18K03579 and JP18H01547, and the Program for Fostering Globally Talented Researchers (JPMXS05G2900001). The authors thank Koki Sugihara for his assistance during the field work.

References

Abe, T., Mizugaki, S., Toyabe, T., Murayama, M., Murakami, Y., and Ishiya, T.: High range turbidity monitoring in the Mu and Saru River Basins: All-year monitoring of hydrology and suspended sediment transport in 2010, International Journal of Erosion Control Engineering, 5(1), 70-79, https://doi.org/10.13101/ijece.5.70, 2012.

Bittelli, M., Flury, M., Campbell, G. S., and Schulz, V.: Characterization of a spiral-shaped time domain reflectometry probe, Water Resources Research, 40, W09205, http://doi.org/10.1029/2004WR003027, 2004.

Buffington, J. M. and Montgomery, D. R.: A systematic analysis of eight decades of incipient motion studies, with special reference to gravel-bedded rivers, Water Resources Research, 33(8), 1993-2029, http://doi.org/10.1029/96WR03190, 1997.

Černý, R.: Time-domain reflectometry method and its application for measuring moisture content in porous materials: A review, Measurement, 42, 329–336, http://doi.org/10.1016/j.measurement.2008.08.011, 2009.

Chung, C.-C. and Lin, C. P.: High concentration suspended sediment measurements using time

410 domain reflectometry, Journal of Hydrology, 401, 123–144,
411 http://doi.org/10.1016/j.jhydrol.2011.02.016, 2011.
412 Chung, C.-C., Lin, C.-P., Wu, P.-L., Hsieh, S.-L., and Wu, C.-H.: Monitoring of Sediment
413 Transport in a Reservoir using Time Domain Reflectometry, in: Proceedings of 2013 IAHR
414 World Congress, Chendu, China, 8-13 September 2013, 1–13, 2013a.
415 Chung, C.-C., Lin, C.-P., Wu, I.-L., Chen, P.-H., and Tsay, T.-K.: New TDR waveguides and data
416 reduction method for monitoring of stream and drainage stage, Journal of Hydrology, 505,
417 346–351, http://doi.org/10.1016/j.jhydrol.2013.09.050, 2013b.
418 Cohen, H. and Laronne, J.B.: High rates of sediment transport by flash floods in the Southern
419 Judean Desert, Israel, Hydrological Processes, 19, 1687–1702.
420 http://doi.org/10.1002/hyp.5630, 2005.
421 Comiti, F., Mao, L., Penna, D., Dell'Agnese, A., Engel, M., Rathburn, S., and Cavalli, M.: Glacier
422 melt runoff controls bedload transport in Alpine catchments, Earth Planetary Science Letters,
423 520, 77–86, http://doi.org/10.1016/j.epsl.2019.05.031, 2019.
424 Dietrich, W. E., Kirchner, J. W., Ikeda, H., and Iseya, F.: Sediment supply and the development
425 of the coarse surface layer in gravel-bedded rivers, Nature, 340, 215–217,
426 http://doi.org/10.1038/340215a0, 1989.
427 Dobson, M. C., Ulaby, F. T., Hallikainen, M. T., and El-Rayes, M. A.: Microwave dielectric
428 behavior of wet soil – Part II: Dielectric mixing models, IEEE Transactions on Geoscience
429 and Remote Sensing, GE-23(1), 35–46, https://doi.org.10.1109/TGRS.1985.289498, 1985.
430 Felix, D., Albayrak, I., and Boes, R.M.: In-situ investigation on real-time suspended sediment
431 measurement techniques: Turbidimetry, acoustic attenuation, laser diffraction (LISST) and
432 vibrating tube densimetry, International Journal of Sediment Research, 33, 3–17,

http://doi.org/ 10.1016/j.ijsrc.2017.11.003, 2018.

García-Mama, A., Pagano, S.G., and Genitle, F.: Suspended sediment transport analysis in two Italian instrumented catchments, Journal of Mountain Science, 13(6), 957–970, http://doi.org/10.1007/s11629-016-3858-x, 2016.

Ghodgaonkar, D. K., Varadan, V. V., and Varadan, V. K.: A free-space method for measurement of dielectric constants and loss tangents at microwave frequencies, IEEE Transactions on Instrumentation and Measurement, 37(3), 789–793, http://doi.org/10.1109/19.32194, 1989.

Gray, J. R. and Gartner, J. W.: Technological advances in suspended-sediment surrogate monitoring, Water Resources Research, 45, W00D29, http://doi.org/10.1029/2008WR007063, 2009.

Heimovaara, T. J. and Bouten, W.: A computer-controlled 36-channel time domain reflectometry system for monitoring soil water contents, Water Resources Research, 26(10), 2311-2316, http://doi.org/10.1029/WR026i010p02311, 1990.

Heimovaara, T. J.: Frequency domain analysis of time domain reflectometry waveforms 1. Measurement of the complex dielectric permittivity of soils, Water Resources Research, 30(2), 189–199, http://doi.org/10.1029/93WR02948, 1994.

Hostache, R., Hissler, C., Matgen, P., Guignard, C. and Bates, P.: Modelling suspended-sediment propagation and related heavy metal contamination in floodplains: A parameter sensitivity analysis, Hydrology and Earth System Sciences, 18, 3539–3551, http://doi.org/10.5194/hess-18-3539-2014, 2014.

Houseknecht, D.: Assessing the relative importance of compaction processes and cementation to reduction of porosity in sandstones, The American Association of Petroleum Geologists Bulletin, 71(6), 633–642, https://doi.org/10.1306/9488787F-1704-11D7-

8645000102C1865D, 1987.

Kociuba, W.: Determination of the bedload transport rate in a small proglacial High Arctic stream using direct, semi-continuous measurement, Geomorphology, 287, 101–115, http://doi.org/10.1016/j.geomorph.2016.10.001, 2017.

Lane, S.N., Tayefi, V., Reid, S.C., Yu, D., and Hardy, R.J.: Interactions between sediment delivery, channel change, climate change and flood risk in a temperate upland environment, Earth Surface Processes and Landforms, 32, 429–446. http://doi.org/10.1002/esp.1404, 2007.

Laronne, J.B., Outhet, D.N., Carling, P.A., and McCabe, T.J.: Scour chain employment in gravel bed rivers, Catena, 22, 299–306, http://doi.org/10.1016/0341-8162(94)90040-X, 1994.

Lenzi, M.A., Mao, L., and Comiti, F.: Interannual variation of suspended sediment load and sediment yield in an alpine catchment, Hydrological Sciences Journal, 48(6), 899–915, http://doi.org/10.1623/hysj.48.6.899.51425, 2003.

Malmberg C.G. and Maryott A.A.: Dielectric constant of water from 0 to 100°C, Journal of Research of the National Bureau of Standards, 56(1), 1–8, 1956.

Martin, Y. and Church, M.: Bed-material transport estimated from channel surveys: Vedder River, British Columbia, Earth Surface Processes and Landforms, 20, 347–361, http://doi.org/10.1002/esp.3290200405, 1995.

Martín-Vide, J.P., Capape, S., and Ferrer-Boix, C.: Transient scour and fill. The case of the Pilcomayo River, Journal of Hydrology, http://doi.org/ 10.1016/j.jhydrol.2019.06.041, 2019.

Mishra, P.N., Bore, T., Jiang, Y., Sheuermann, A., and Li, L.: Dielectric spectroscopy measurements on kaolin suspensions for sediment concentration monitoring, Measurement, 121, 160–169. http://doi.org/10.1016/j.measurement.2018.02.034, 2018.

Miyata, S. and Fujita, M.: Laboratory experiment of continuous bedload monitoring at the

479 retention basin of a steep mountain river, Earth Surface Processes and Landforms, 43, 2022–
480 2030, http://doi.org/ 10.1002/ esp.4358, 2018.
481 Mizugaki S., Abe, T., Murakami, Y., Maruyama, M., and Kubo, M.: Fingerprinting suspended
482 sediment sources in the Nukabira River, northern Japan, International Journal of Erosion
483 Control Engineering, 5(1), 60–69, http://doi.org/10.13101/ijece.5.60, 2012.
484 Mizugaki, S., Maruyama, M., Watanabe, K., Yabe, H., and Abe, T.: Field observation of
485 suspended sediment using turbidity probe in a cold snowy mountain catchment, Proceedings
486 of the Japan Society of Erosion Control Engineering Annual Conference 2013, R1-10, 2013.
487 (in Japanese)
488 Nissen, H. H., Moldrup, P., and Henriksen, K.: High-resolution time domain reflectometry coil
489 probe for measuring soil water content, Soil Science Society of America Journal, 62, 1203–
490 1211, http://doi.org/10.2136/sssaj1998.03615995006200050008x,1998.
491 Noborio K.: Measurement of soil water content and electrical conductivity by time domain
492 reflectometry: A review, Computers and Electronics in Agriculture, 31, 213–237,
493 http://doi.org/10.1016/S0168-1699(00)00184-8, 2001.
494 Núñez-González F.: Infiltration of fine sediment mixtures through poorly sorted immobile coarse
495 beds, Water Resources Research, 52, 9306–9324, http://doi.org/10.1002/2016WR019395,
496 2016.
497 Persson, M. and Dahlin, T.: A profiling TDR probe for water content and electrical conductivity
498 measurements of soils, European Journal of Soil Science, 61, 1106–1112,
499 http://doi.org/10.1111/j.1365-2389.2010.01306.x, 2010.
500 Piqué, G., Batallaa, R.J., López, R., and Sabatera, S.: The fluvial sediment budget of a dammed
501 river (upper Muga, southern Pyrenees), Geomorphology. 293, 211–226,

http://doi.org/10.1016/j.geomorph.2017.05.018, 2017.

Rai, A.K. and Kumar, A.: Continuous measurement of suspended sediment concentration: Technological advancement and future outlook, Measurement, 76, 209–227, http://dx.doi.org/10.1016/j.measurement.2015.08.013, 2015.

Robinson, D.A. and Friedman, S.P.: A method for measuring the solid particle permittivity or electrical conductivity of rocks, sediments, and granular materials, Journal of Geophysical Research, 108(B2), 2076, http://doi.org/10.1029/2001JB000691, 2003.

Starr, G.C., Barak, P., Lowery, B., and Avila-Segura, M.: Soil particle concentrations and size analysis using a dielectric method. Soil Sciences Society of America Journal, 64, 858–866, http://doi.org/10.2136/sssaj2000.643858x, 2000.

Starr, G.C.: Basal sediment concentration measurement using a time domain reflectometry method, Transactions of the American Society of Agricultural Engineering, 48(1), 205–209, http://doi.org/10.13031/2013.17964, 2005.

Topp, G. C., Davis, J. L., and Annan, A. P.: Electromagnetic determination of soil water content: Measurements in coaxial transmission lines, Water Resources Research, 16(3), 574–582, http://doi.org/10.1029/WR016i003p00574, 1980.

Turowski, J.M., Rickenmann, D., and Dadson, S.J.: The partitioning of the total sediment load of a river into suspended load and bedload: a review of empirical data, Sedimentology, 57, 1126–1146, http://doi.org/ 10.1111/j.1365-3091.2009.01140.x, 2010.

Voichick, N., Topping, D.J., and Griffiths, R.E.: Technical note: False low turbidity readings from optical probes during high suspended-sediment concentrations, Hydrology and Earth System Sciences, 22, 1767–1773, http://doi.org/10.5194/hess-22-1767-2018, 2018.

Walling, D.E. and Collins, A.L.: The catchment sediment budget as a management tool,

Environmental Science & Policy, 11, 136–143, http://doi.org/10.1016/j.envsci.2007.10.004, 2008.

Walling, D.E., Owens, P.N., Waterfall, B.D., Leeks, G.J.L., and Wass, P.D.: The particle size characteristics of fluvial suspended sediment in the Humber and Tweed catchments, UK, The Science of the Total Environment, 251–252, 205–222, http://doi.org/10.1016/S0048-9697(00)00384-3, 2000.

Woodhead, I.M., Buchan, G.D., Christie, J.H., and Irie, K.: A general dielectric model for time domain reflectometry, Biosystems Engineering, 86(2), 207–216, http://doi.org/10.1016/S1537-5110(03)00131-4, 2003.

Wren, D. G., Barkdoll, B. D., Kuhnle, R. A., and Derrow, R. W.: Field techniques for suspended-sediment measurement, Journal of Hydraulic Engineering, 126(2), 97–104, https://doi.org/10.1061/(ASCE)0733-9429(2000)126:2(97), 2000.

Table 1 Calibrated values of actual probe length and coefficient values for the effect of PVC pipe.

Probe	L **[m]**	α **[-]**
A	1.14	0.252
B	1.13	0.244
C	1.15	0.257
D	1.13	0.263
E	1.13	0.251

Table 2 Sand and probe types used in the experiments.

		Sand	Median diameter [mm]	TDR probe
Experiment I				A, B, C, D, E
Experiment II				
	Run II-1	Silica Sand #7	0.2	A, B, C, D, E
	Run II-2	Kaolin clay	0.0004	B, C, D

Table 3 Results of regression analysis for Experiment II

	Run II-1			Run II-2		
	$C_{TDR} = a + bC$			$C_{TDR} = a + bC$		
	a	b	r^2	A	b	r^2
Coil A	-0.0021	1.05	0.97			
Coil B	-0.0008	1.05	0.98	-0.0039	0.979	1.00
Coil C	0.0047	0.882	0.88	0.0078	0.807	0.97
Coil D	-0.0062	0.852	0.93	0.0217	0.837	0.96
Coil E	0.0031	1.02	0.99			
3-rod type	0.0131	0.700	0.95	0.0162	0.834	0.99

Table 4 Analysis of covariance (ANCOVA) of averaged SCs for each concentration level of Run II-1 and Run II-2

	Degree of freedom	Sum of squares	Mean square	F value	P value
Group	1	0.0000604	0.0000604	4.161	0.054
Error	21	0.000305	0.0000145		

548

549

550

Fig. 1

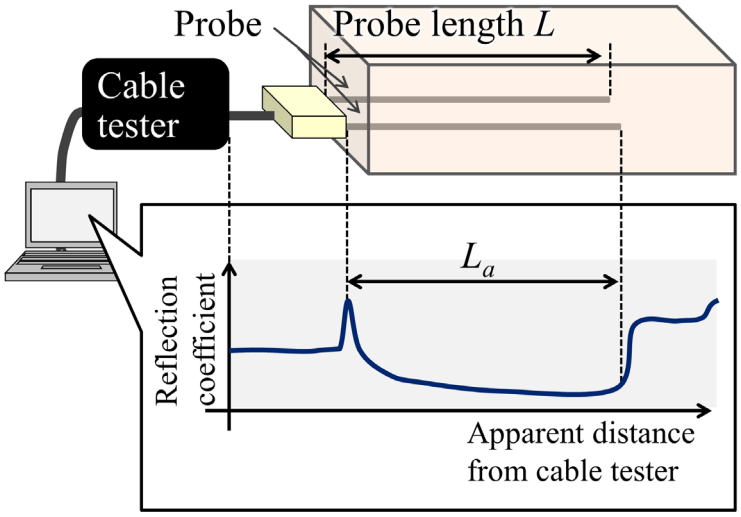

551

552 Fig. 1 Schematic of the measurement system and the primary measurement results.

Fig. 2

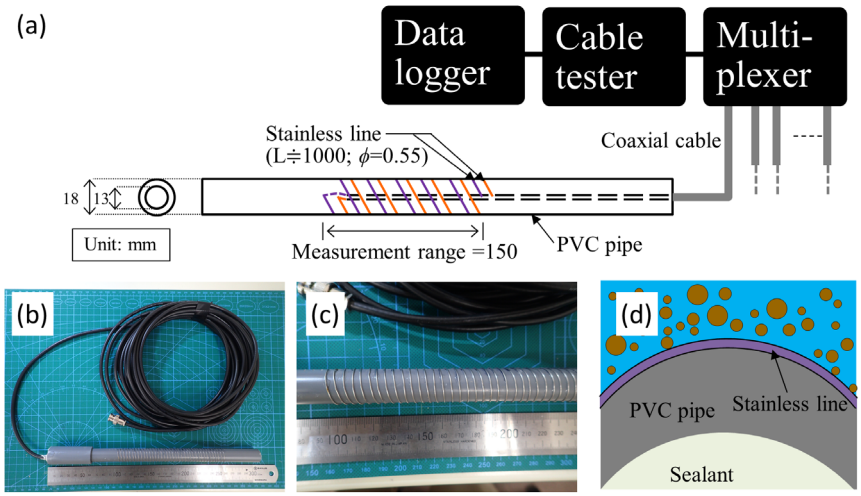

553

554 Fig. 2 (a) Schematic of the time domain reflectometry (TDR) measurement system with a coil-
555 type probe, (b and c) photographs of the coil-type probe and (d) schematic of the cross
556 section of a probe.

Fig. 3

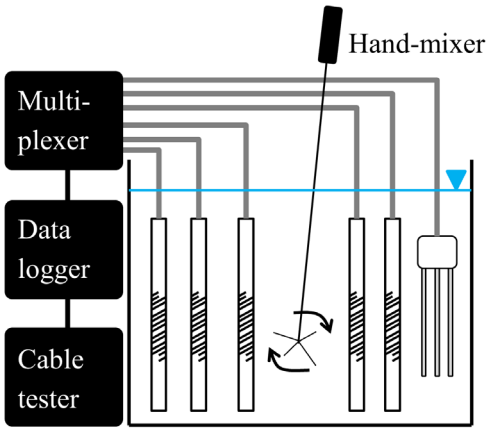

557

558 Fig. 3 Schematics of (a) Experiment II and (b) Experiment III.

Fig. 4

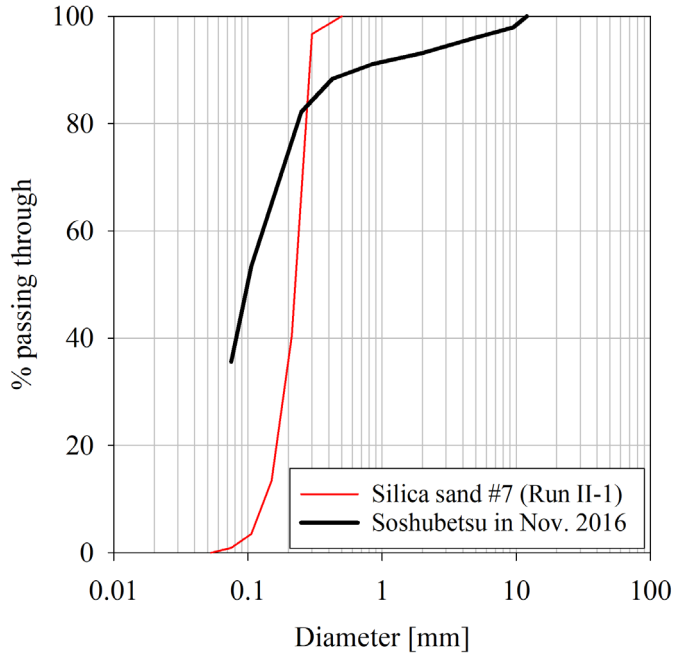

559

560 Fig. 4 Grain size distributions of sands used in the experiments and a stream bed sample collected

561 from the study site in November 2016.

Fig. 5

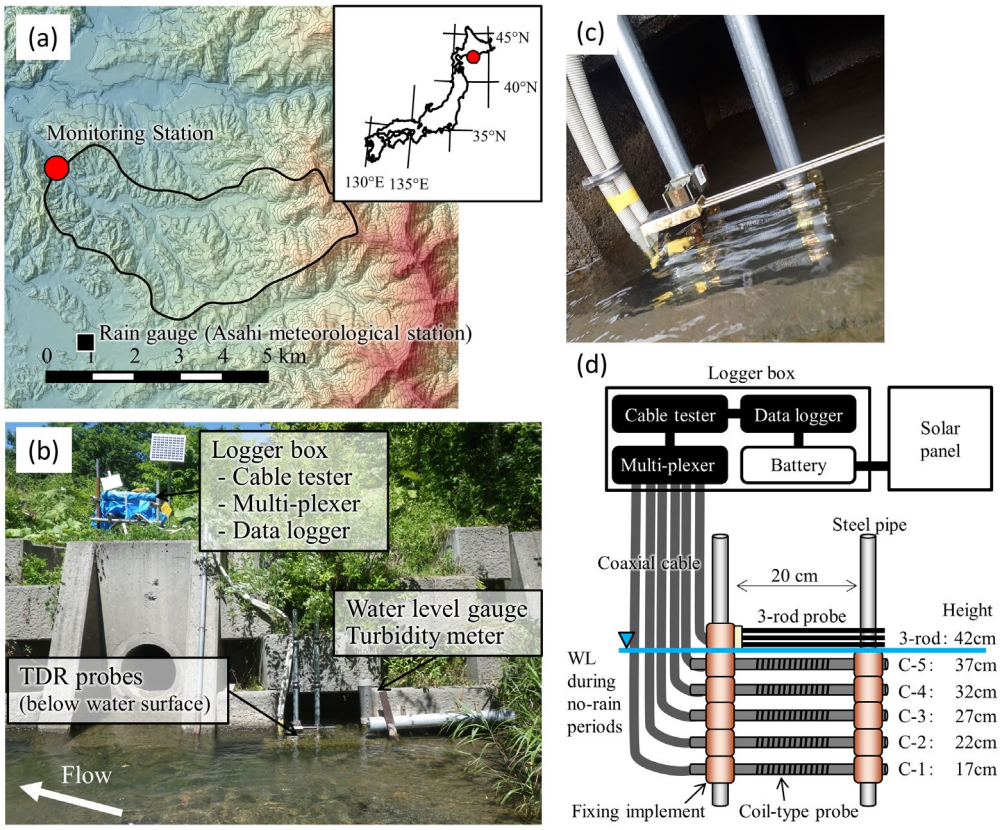

562

563 Fig. 5 (a) Location of the study site, (b and c) photographs of the monitoring station and

564 the installed time domain reflectometry (TDR) probes and (d) schematic of the TDR

565 measurement system in the monitoring station.

Fig. 6

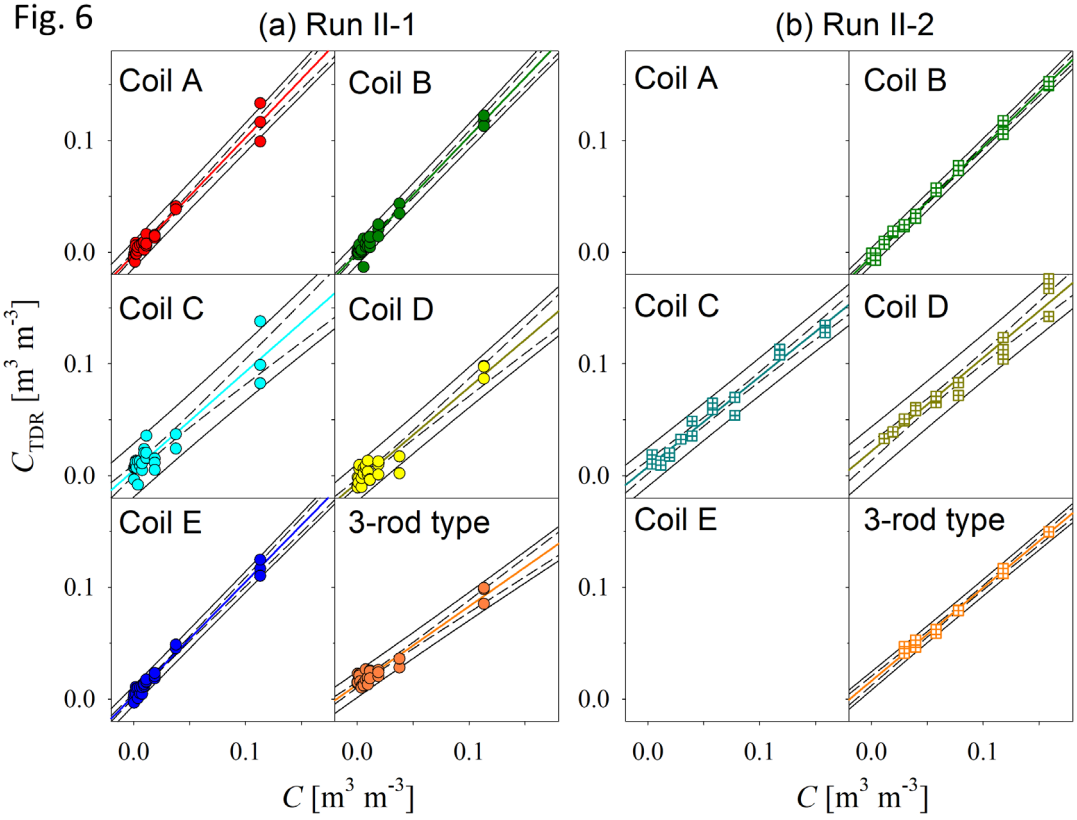

566

567 Fig. 6 The relationships between actual sediment concentration (C) and sediment concentration
568 measured using the time domain reflectometry (TDR) system developed in this study
569 (C_{TDR}). Coloured, solid, and broken lines indicate regression line, 95% confidence interval,
570 and 95% prediction interval, respectively.

Fig. 7

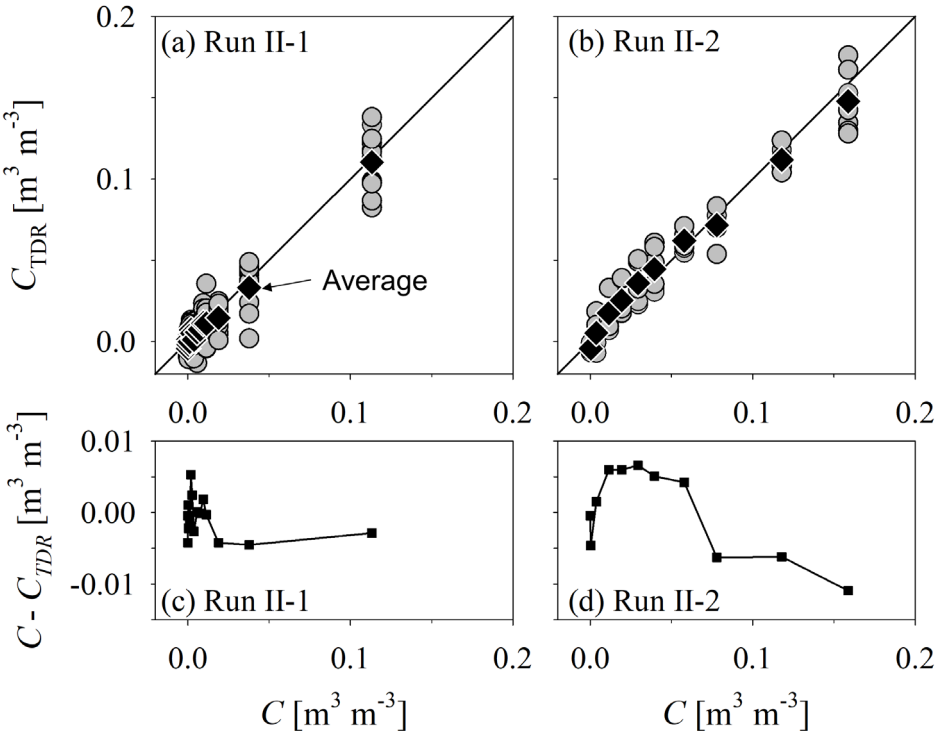

571

572 Fig. 7 The relationships between actual sediment concentration (C) and measured sediment
573 concentration (C_{TDR}) in (a) Run II-1 and (b) Run II-2, and the relationships between actual
574 sediment concentration and C-C_{TDR} in (c) Run II-1 and (d) Run II-2.

Fig. 8

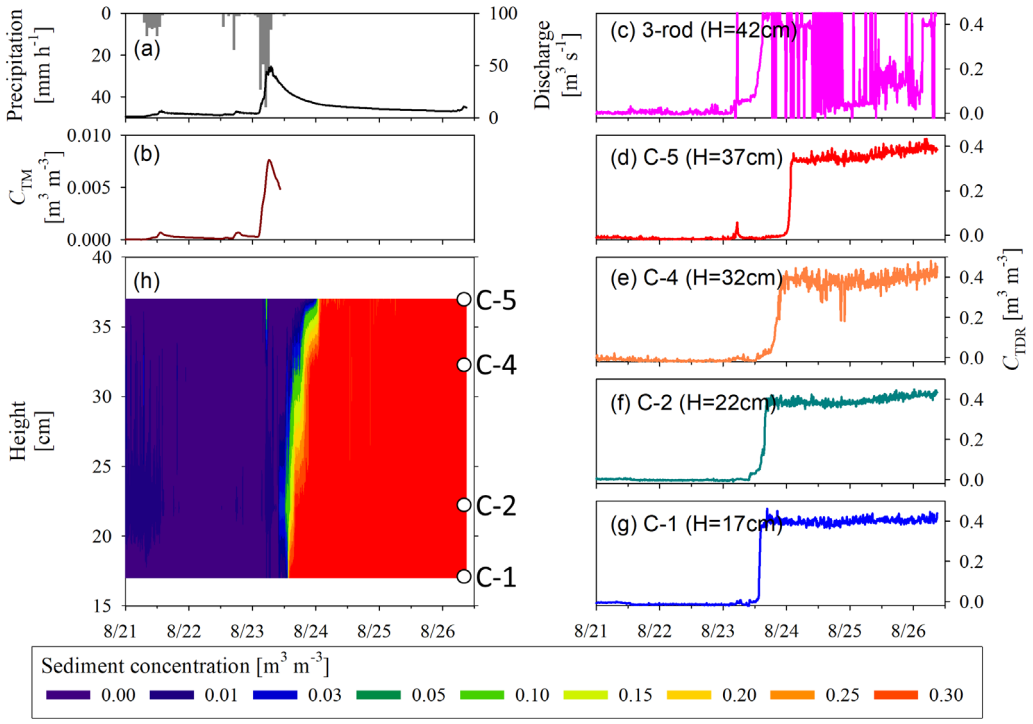

575

576 Fig. 8 (a) Temporal changes in precipitation and stream discharge. (b) Sediment concentrations
577 measured by a turbidity meter (C_{TM}). (c–g) Time domain reflectometry (TDR) at heights of
578 17–42 cm (C_{TDR}). (h) Vertical distributions of sediment concentration during a storm event
579 from 21 to 25 August 2016. The concentration distributions shown as coloured contours
580 are provided at the bottom of the figure. Open circles in Fig. 11h indicate probe heights.

Fig. 9

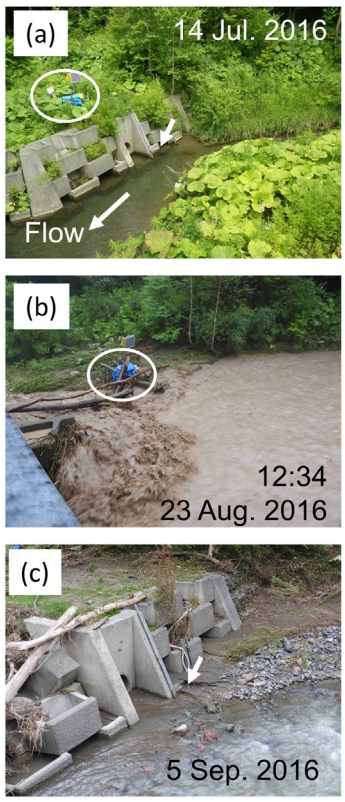

581

582 Fig. 9 Photographs of the monitoring station (a) at the beginning of the observation, and (b) during
583 and (c) after a flooding event. White circles and white arrows indicate the locations of the
584 logger box and probes of the time domain reflectometry (TDR) system, respectively.

Fig. 10

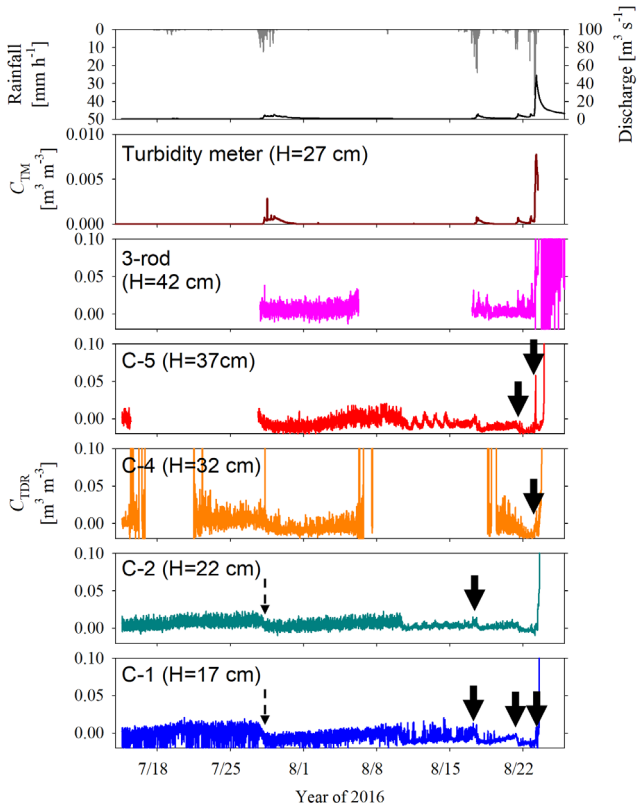

585

586 Fig. 10 Temporal changes in precipitation, stream discharge and sediment concentrations
587 measured by a turbidity meter (C_{TM}) and time domain reflectometry (TDR) at heights of
588 17-42 cm (C_{TDR}) during the monitoring period.

Fig. 11

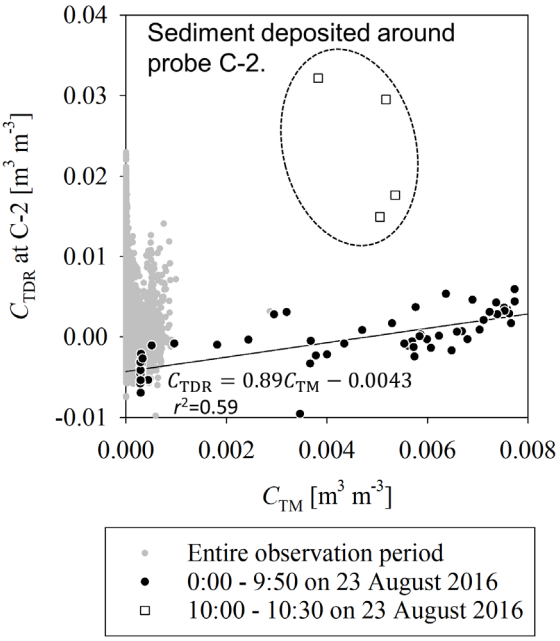

589

590 Fig. 11 Comparison between the volumetric sediment concentrations measured by probe C-2
591 (C_{TDR}) and the turbidity meter (C_{TM}). A solid line indicates the regression line for data from
592 0:00-9:50 on 23 August 2016.

Fig. 12

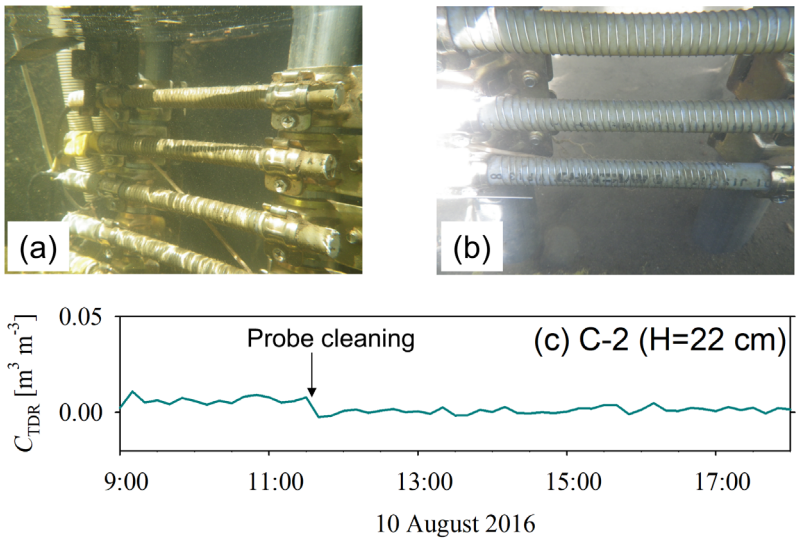

593

594 Fig. 12 Photographs of the probes in the stream (a) before and (b) after cleaning and (c)

595 sediment concentration measured at probe C-2 on 10 August 2016.

596

597

598

599

600

601